Hydrodynamic modeling of charge carrier transport and transverse pattern formation in ZnS:Mn thin-film electroluminescent structures

K. Meyer,[1] T. Raker,[2] F.-J. Niedernostheide,[2] and T. Kuhn[1]
[1]*Institut für Festkörpertheorie, Westfälische Wilhelms-Universität Münster, Wilhelm-Klemm-Strasse 10, 48149 Münster, Germany*
[2]*Infineon Technologies AG, 81726 München, Germany*
(Received 13 June 2007; revised manuscript received 19 October 2007; published 18 January 2008)

The charge carrier transport and transverse pattern formation in ac-driven thin-film electroluminescent devices are studied on a hydrodynamic level. A set of model equations is set up to describe the coupled dynamics of the charge carriers and the local lattice temperature. Assuming a laterally homogeneous system, the number and stability of stationary states is analyzed in one-dimensional simulations. Starting from laterally inhomogeneous initial conditions, the formation and dynamics of transverse patterns is studied in two-dimensional simulations. The influence of frequency and amplitude of the applied voltage as well as of the relative time scales of thermal and electrical transport on the results is investigated. Depending on the parameters, we find a variety of different patterns, such as localized high- or low-current filaments, temporally or spatially oscillating solutions, and moving high-field domains. The results are interpreted on the basis of null cline diagrams for the space charge and lattice temperature dynamics. The two-dimensional patterns are compared to luminescence patterns that were found in various experiments.

DOI: 10.1103/PhysRevB.77.045321 PACS number(s): 73.50.Fq, 73.40.Qv, 73.43.Cd, 05.45.Ac

I. INTRODUCTION

Thin-film structures made of a wide band gap semiconductor layer, which is doped with luminescence centers and sandwiched between two insulating layers, are both of basic physical interest and of technological relevance. When driven by a sufficiently high ac voltage, such metal-insulator-semiconductor-insulator-metal (MISIM) devices emit light, the color of which can be controlled by doping with specific impurity centers such as Mn or Cr. This light emission is the basis for their application, e.g., in flat-panel displays.[1] Due to the high electric fields, these systems are driven very far from thermal equilibrium. In particular, in the transition region between the dark state at low voltages and the bright state at high voltages, it has been found that they exhibit a variety of spatiotemporal light-density and current-density structures (see, e.g., Refs. 2–8), which makes them attractive candidates for the study of nonlinear pattern formation phenomena in solid state systems.

Pattern formation phenomena in semiconductors depend on the type of the nonlinearity in the current-voltage characteristic.[9] In the case of an N-shaped characteristic, typically, a formation of static or dynamic domains in the longitudinal direction, i.e., in the direction of the current flow, is observed. Prominent examples for this case are semiconductor superlattices, where the N shape results from the tunneling characteristic through the barriers.[10–13] In contrast, an S-shaped current-voltage characteristic, as it occurs in thin-film electroluminescent devices, typically leads to pattern formation in the directions transverse to the current flow. Such an *S* shape is often based on impact ionization processes, and generic patterns are static or dynamic current filaments or fronts.[14–16] In ac-driven ZnS:Mn films, a particularly rich scenario of such transverse patterns has been observed, which includes, in addition to filaments and fronts, also structures such as autowaves, spiral waves, and target patterns.[4,6,7,17]

The theoretical modeling of pattern formation phenomena in ac-driven MISIM structures, starting from the fundamental semiconductor transport processes, faces severe difficulties arising from strongly different length and time scales entering the carrier transport and the pattern formation dynamics. A basic ingredient for the simulation of transverse pattern formation is an accurate model for the longitudinal charge carrier transport between the two electrodes since this is the main transport direction. There have been several approaches[18–23] to model the longitudinal transport in such thin-film devices. They all rely on the same basic assumptions on the relevant processes: Carriers are released from interface states at the insulator-semiconductor interface by tunneling in the high electric fields, impact ionization processes result in a multiplication of the injected carriers, and the capture of some part of the free carriers by localized traps leads to the buildup of a space charge.

Howard, Sahni, and Alt[18] presented the first model for the one-dimensional transport in a ZnS:Mn MISIM structure (HSA model). For the tunnel injection current, they applied an expression resulting from a Wentzel-Kramers-Brillouin (WKB) approximation, and the impact ionization (II) coefficient was modeled by an analytical formula that exhibited a pronounced threshold. A drawback of this model is that the field dependence of this II coefficient is much steeper than either experiments[24] or recent Monte Carlo simulations[25] would suggest. A second drawback, which is even more essential for our present purposes, is based in the structure of the model: Because of the reduction of the drift-diffusion model to a first order differential equation for the current density, it cannot be extended to more than one spatial dimension, and so transverse pattern formation cannot be explained on the basis of the HSA model.

In a previous paper,[26] we have studied the one-dimensional transport on the basis of a full hydrodynamic model including electron injection from interface states, band-to-band impact ionization, hole trapping, and thermal

reemission of trapped holes into the valence band. The calculations have been performed by using three different models for the II coefficient. Besides the shape taken in the HSA model, we also used the field dependences extracted form the experiments by Thompson and Allen[24] and from the Monte Carlo simulation by Kuligk *et al.*[25] From the calculations, we have extracted the average electric current as a function of the amplitude and frequency of the applied voltage. For all three II models, the system exhibited a bistable behavior in wide parameter ranges. Furthermore, the results showed that, as could be expected from the extremely high electric fields, very high carrier temperatures are reached. However, because of the small values of the heat conductivity resulting from the low densities of free carriers and because of the small gradients in the electron and hole current densities, heat transport effects described by gradients of the energy current densities turned out to be negligible. This allowed us to effectively reduce the hydrodynamic transport model to a drift-diffusion-like model, but with spatially and temporally varying carrier temperatures.

The model presented in this paper is based on the model given in Ref. 26 but extended to two spatial dimensions, the longitudinal (z) and one lateral (x) direction. For a hydrodynamic or drift-diffusion model, such an extension is straightforward. Nevertheless, it strongly increases the numerical effort mainly because of the long times that have to be simulated. In addition, the model has been extended by including the local lattice temperature as a dynamical variable. It can be expected that due to the strong driving, the Joule heating increases the device temperature—especially when operating at high frequencies—which results in a reduction of the space charge due to an increased thermal emission of trapped holes.[4,27,28] To model this behavior, we have added a transport equation for the lattice temperature with an Ohmic heat source and have considered a thermally activated emission process of holes from hole traps.

Based on this model, we have calculated the stable periodic stationary states of the laterally homogeneous system, i.e., the states where the system after one period of the driving voltage is unchanged, for different amplitudes and frequencies of the applied voltage. Since even in the bistable regime in most cases the laterally homogeneous state is stable with respect to small perturbations, numerical uncertainties are not sufficient to obtain laterally inhomogeneous states. Therefore, in order to obtain the formation of transverse patterns, some kind of seed is necessary. In the present case, we have prepared such a seed by an inhomogeneous initial condition where we have put some part of the device on the lower branch and another part on the upper branch of the hysteresis loop. We have checked that also by adding some static or dynamic noise to the simulations modeling device imperfections, which are always present in a real structure, the same patterns are obtained, but in a much less controllable way and sometimes only after very long simulation times.

II. TRANSPORT MODEL

In this paper, we study a MISIM structure identical to the one discussed in Ref. 26, which is shown in Fig. 1. In such a structure, various spatiotemporal patterns have been observed experimentally.[6,17] It consists of a manganese doped ZnS layer, which is sandwiched between two insulating $BaTiO_3$ layers. On one side, it is contacted by an aluminum layer, and on the other side by a transparent indium-tin-oxide contact so that the emitted light patterns can be observed with the help of a microscope. In the calculation, we include the longitudinal (z) and one transverse (x) direction of the device.

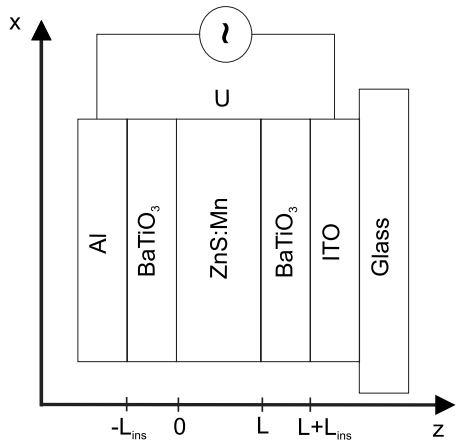

FIG. 1. Scheme of the MISIM structure with the semiconductor ZnS:Mn layer, two insulating layers of $BaTiO_3$, an aluminum contact on one side, a transparent indium-tin-oxide contact on the other side, and a glass substrate.

A. Transport equations

To model the carrier dynamics, we use a two-dimensional version of the hydrodynamic model presented in Ref. 26, where a detailed discussion of the one-dimensional (longitudinal) charge carrier dynamics can be found. Here, we want to give a brief summary of the equations used in the present case and to discuss the extensions and modifications with respect to our previous studies. The main physical processes considered are the field-induced tunnel injection of electrons from surface states at the semiconductor-insulator interface to the conduction band, recombination with interface states on the opposite side, and electron-hole pair generation by impact ionization. The generated holes can be trapped and re-emitted by hole traps. In addition to our previous studies, we now include the heating of the crystal lattice due to Ohmic heating, which affects the emission process of trapped holes to the valence band.

The time constants, which define the drift and diffusion velocities of free holes and electrons, are much smaller than the time scales on which the trapped holes, the surface charge density, and the external forces are changing. This means that for a given space charge profile, given surface charge densities on the left and right interfaces, and a given value of the applied external voltage, the free carrier densities can be considered as stationary. For this reason, the time derivatives in the transport equations for the free carriers can be neglected. With the additional approximation of neglecting the heat transport terms, which has been checked and

justified in Ref. 26, the resulting hydrodynamic transport equations for electrons and free holes are given by

$$0 = -\nabla \cdot \mathbf{j}_n + G_{\mathrm{II}} - R_{np} - R_{nt}, \tag{1}$$

$$\mathbf{j}_n = -D_n n \nabla \left(\frac{T_n}{T_0}\right) - D_n \frac{T_n}{T_0} \nabla n + \mu_n n \nabla \varphi, \tag{2}$$

$$0 = e\mathbf{j}_n \cdot \nabla\varphi - \frac{3}{2} n \frac{k_B}{\tau_n^E}(T_n - T_L) + G_n^{(2)} \tag{3}$$

and

$$0 = -\nabla \cdot \mathbf{j}_p + G_{\mathrm{II}} - R_{np} - R_{pt}, \tag{4}$$

$$\mathbf{j}_p = -D_p p \nabla \left(\frac{T_p}{T_0}\right) - D_p \frac{T_p}{T_0} \nabla p - \mu_p p \nabla \varphi, \tag{5}$$

$$0 = -e\mathbf{j}_p \cdot \nabla\varphi - \frac{3}{2} p \frac{k_B}{\tau_p^E}(T_p - T_L) + G_p^{(2)}. \tag{6}$$

Here, n, $\mathbf{j}_n$, and T_n (p, $\mathbf{j}_p$, and T_p) denote the density, current density, and temperature of the electrons (free holes), respectively, φ is the electrostatic potential, $D_{n,p} = \frac{k_B T_0}{e}\mu_{n,p}$ are the diffusion constants at the reference temperature $T_0 = 300$ K, and k_B and e denote Boltzmann's constant and the elementary charge, respectively. The energy relaxation times of electrons and holes $\tau_{n,p}^E = \tau_0 T_{n,p}/T_0$ are chosen to be temperature dependent, as proposed by Lundstrom.[29] In order to take the velocity saturation effect of the carrier velocities at high electric fields into account, we use standard field dependent mobilities given by

$$\mu_{n,p}(E) = \frac{\mu_{n,p}^0}{\sqrt{1 + \left(\frac{\mu_{n,p}^0 E}{v_{n,p}^s}\right)^2}}, \tag{7}$$

with the low field mobilities $\mu_{n,p}^0$ and the saturation velocities of electrons and holes $v_{n,p}^s$. The terms G_{II}, R_{np}, R_{nt}, R_{pt}, and $G_{n,p}^{(2)}$ describe generation and recombination rates, which will be specified below.

For the carrier system, there are thus only three transient equations left, which have to be integrated in time. These are the equations for the trapped hole density p_t and for the interface charge densities $\rho_{l,r}$ at the left and right semiconductor-insulator interfaces given by

$$\frac{\partial p_t(x,z,t)}{\partial t} = R_{pt}(x,z,t) - R_{nt}(x,z,t), \tag{8}$$

$$\frac{\partial \rho_l(x,t)}{\partial t} = -\sigma_n[n(x,0,t) - n_0] + \sigma_p[p(x,0,t) - p_0] + j_t^l(x,t), \tag{9}$$

$$\frac{\partial \rho_r(x,t)}{\partial t} = -\sigma_n[n(x,L,t) - n_0] + \sigma_p[p(x,L,t) - p_0] - j_t^r(x,t). \tag{10}$$

Here, $\sigma_{n,p}$ are the surface recombination velocities of electrons and holes, n_0 and p_0 are the thermal equilibrium values of the electron and free hole densities, and $j_t^{l,r}$ are the injected tunnel current densities at the respective interfaces.

This system of equations for the charge carrier distributions has to be solved together with Poisson's equation,

$$\Delta\varphi = -\frac{e}{\epsilon_r \epsilon_0}(p_t + p - n + \rho_l \delta(z) + \rho_r \delta(z - L)), \tag{11}$$

with the vacuum permittivity ϵ_0 and the dielectric permittivity ϵ_r, which is 14 in the insulator and 8 in the semiconductor.

To model the self-heating effect of the MISIM device, in particular, at high frequencies of the applied voltage, we extend the model by including a transport equation for the lattice temperature T_L with an Ohmic heat source according to

$$\frac{\partial}{\partial t} T_L = D_L \Delta T_L + \frac{e}{c_L \rho}(\mathbf{j}_p - \mathbf{j}_n) \cdot \mathbf{E}, \tag{12}$$

with the temperature diffusion constant $D_L = \kappa/(\rho c_L)$, the lattice heat conductivity κ, the heat capacity c_L, and the material density ρ.

B. Boundary conditions

The transport equations have to be completed by boundary conditions. In the longitudinal z direction, we use the same boundary conditions as in the one-dimensional calculations.[26] For the electrons, they describe the processes of surface recombination and tunnel injection while for the free holes, only surface recombination is present, resulting in the following equations for the normal components of the current densities:

$$j_{n,z}(x,0,t) = -\sigma_n[n(x,0,t) - n_0] + j_t(x,t),$$

$$j_{n,z}(x,L,t) = \sigma_n[n(x,L,t) - n_0] - j_t(x,t),$$

$$j_{p,z}(x,0,t) = -\sigma_p[p(x,0,t) - p_0],$$

$$j_{p,z}(x,L,t) = \sigma_p[p(x,L,t) - p_0].$$

The electrostatic potential at the contacts ($z = -L_{\mathrm{ins}}$ and $z = L + L_{\mathrm{ins}}$) is given by the time-dependent applied voltage $V(t) = U\cos(2\pi f t)$, with amplitude U and frequency f according to

$$\varphi(x, -L_{\mathrm{ins}}, t) = V(t), \quad \varphi(x, L + L_{\mathrm{ins}}, t) = 0.$$

The boundary conditions for the lattice temperature at $z = -L_{\mathrm{ins}}$ and $z = L + L_{\mathrm{ins}}$ are modeled by a thermal resistance $1/\eta$ according to

$$D_L \frac{\partial}{\partial z} T_L(x, -L_{\mathrm{ins}}, t) = \eta[T_L(x, -L_{\mathrm{ins}}) - T_0],$$

$$D_L \frac{\partial}{\partial z} T_L(x, L + L_{\text{ins}}, t) = -\eta [T_L(x, L + L_{\text{ins}}, t) - T_0].$$

In the lateral x direction, we use periodic boundary conditions for all variables to avoid unwanted boundary effects in this direction.

C. Rates

The impact ionization rate G_{II} is taken to be the product of electron current density and a field dependent impact ionization coefficient $\alpha(E)$. In this paper, we use a field dependence of α, which was calculated by Redmer, Kuligk, and Fitzer from Monte Carlo simulations[25,30] and is shown in Ref. 26 as the RKF coefficient. Also the WKB expression used for the tunnel current density can be found in Ref. 26.

For the recombination processes of free electrons with trapped and free holes, we apply the rates

$$R_{np} = \gamma_{np}(np - n_0 p_0), \tag{13}$$

$$R_{nt} = \gamma_{nt}(np_t - n_0 p_{t0}), \tag{14}$$

with the recombination coefficients γ_{np} and γ_{nt} and the thermal equilibrium values of the trapped hole density p_{t0}. The process of hole trapping and emission is expressed by

$$R_{pt} = \gamma_c(N_t - p_t)p - \gamma_e(T_L)p_t, \tag{15}$$

where γ_c is the hole capture coefficient, γ_e the hole emission rate, and N_t the density of trap centers. The lattice temperature dependence of γ_e can be expressed as[31]

$$\gamma_e(T_L) = \gamma_c N_v \exp\left(\frac{E_t - E_v}{k_B T_L}\right), \tag{16}$$

with the effective density of energy levels for the valence band N_v, the energy level of the valence band edge E_v, and the energy level of the traps E_t. This is consistent with an expression given by Vlasenko *et al.*,[27] which is justified by measurements of the temperature dependence of the hysteresis widths. Using $\Delta E = E_t - E_v$, Eq. (16) can be rewritten in a form that contains the emission rate $\tilde{\gamma}_e$ at $T_L = 300$ K,

$$\gamma_e(T_L) = \tilde{\gamma}_e \exp\left[\frac{\Delta E}{k_B T_0}\left(1 - \frac{T_0}{T_L}\right)\right]. \tag{17}$$

The temperature dependence of all other coefficients is much weaker and is therefore neglected in the calculations.

The material and structure parameters that have been used in the simulations are summarized in Table I. In the z direction, we have used a nonuniform discretization grid of 70 points, and in the x direction, it turned out that at least 64 points per 10 μm are needed. For each period of the applied voltage, we used 100 time steps.

TABLE I. Material and structure parameters used in the simulations.

Parameter	Value
Insulator width	$L_{\text{ins}} = 300$ nm
ZnS-layer width	$L = 500$ nm
Surface recombination velocities	$\sigma_n = 10^7$ cm/s
	$\sigma_p = 10^7$ cm/s
Low field mobilities	$\mu_n^0 = 165$ cm^2/V s[a]
	$\mu_p^0 = 5$ cm^2/V s[a]
Maximum drift velocity	$v_n^s = 2 \times 10^7$ cm/s[b]
	$v_p^s = 2 \times 10^7$ cm/s
Energy relaxation time	$\tau_0 = 10^{-13}$ s
Hole trap density	$N_t = 10^{17}$ cm^{-3}
Hole capture coefficient	$\gamma_c = 10^{-6}$ cm^3/s
Hole emission rate at 300 K	$\tilde{\gamma}_e = 10^2$ s^{-1}
Specific heat capacity	$c_L = 500$ J/kg K
Material density	$\rho = 4$ g/cm^3
Lattice heat conductivity	$\kappa = 17$ W/m K
Inverse thermal resistance	$\eta = 40.0$ m/s
Trap energy level ($E_t - E_v$)	$\Delta E = 0.5$ eV[c]

[a]Reference 32.
[b]Reference 33.
[c]Reference 27.

III. RESULTS

A. Constant lattice temperature

Before analyzing the full dynamics of the carrier system coupled to the lattice temperature, in this section, we shall briefly discuss the behavior of the system at different but constant lattice temperatures T_L. The results will show how the lattice temperature affects the carrier dynamics; therefore, they will be the basis for the interpretation of the behavior of the full model in the following sections.

From our previous studies,[26] we know that in a certain parameter range (determined by the amplitude and the frequency of the driving voltage), the one-dimensional transport exhibits a bistable behavior. The average current as a function of the voltage amplitude is characterized by a hysteresis loop with a lower and an upper branch in a certain range of voltages. If we extend such a bistable system to two dimensions, a natural question arises: What happens if spatially inhomogeneous initial conditions are given? The simplest inhomogeneous case is a situation where one part of the simulated area is set to the high state, which is defined by high densities of trapped holes and surface charges $p_t(z) = p_t^h(z)$, $\rho_{l,r} = \rho_{l,r}^h$, while the other is set to the low state with low carrier densities $p_t(z) = p_t^l(z)$, $\rho_{l,r} = \rho_{l,r}^l$. Thus, the initial conditions can be written as

$$p_t^0(x,z) = \begin{cases} p_t^l(z) & : \quad x \notin X \\ p_t^h(z) & : \quad x \in X, \end{cases} \tag{18a}$$

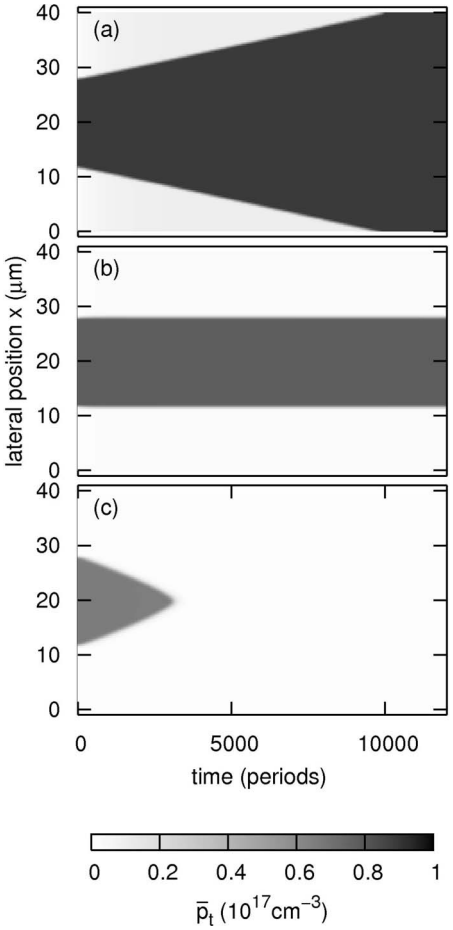

FIG. 2. Temporal evolution of $\bar{p}_t(x,t)$ starting from an inhomogeneous initial conditions for three different lattice temperatures: (a) T_L=280 K, (b) T_L=305 K, and (c) T_L=315 K. The lattice temperature has been taken to be constant. Driving voltage: U =110 V, f=10 kHz.

$$\rho_{l,r}^{0}(x) = \begin{cases} \rho_{l,r}^{l} & : \quad x \notin X \\ \rho_{l,r}^{h} & : \quad x \in X, \end{cases} \tag{18b}$$

with some interval X. In this section, X is chosen to be X =[12 μm,28 μm] for a full lateral width of the simulated device of 40 μm.

The temporal evolution of the trapped hole density spatially averaged over the thickness L of the ZnS layer and temporally averaged over a driving period τ,

$$\bar{p}_t(x,t) = \frac{1}{L\tau}\int_t^{t+\tau} dt' \int_0^L dz p_t(x,z,t'), \tag{19}$$

for such initial conditions is shown in Fig. 2 as a function of time and the lateral coordinate x for three different values of the lattice temperature. Black corresponds to high densities of trapped holes, i.e., to regions of the structure on the upper branch of the hysteresis loop, and white to low densities, i.e., to regions on the lower branch. In Fig. 2(a), which shows the result for a lattice temperature of T_L=280 K, we see that the high-state area increases with time and, after a certain number of periods, covers the whole simulated area. Figure 2(c) shows the behavior at a lattice temperature of T_L=315 K. Now, we find that the low-state area propagates until it covers the entire system. Thus, obviously, the velocity v of the fronts, which separate the high-state area from the low-state area, is a function of the lattice temperature and changes its sign at a temperature of approximately 305 K, as can be seen in Fig. 2(b). One can calculate the lattice temperature at which the front velocity vanishes for every frequency and amplitude of the driving voltage, and we will call this the v=0 temperature in further discussions.

To explain the moving fronts and the lattice temperature dependence of the front velocity, we need to know how the stationary states of the system depend on the lattice temperature. Here—as in the following—stationary means that the system does not change from one period to another. Of course, within one period, there is still a time dependence of the variables. To obtain this temperature dependence, we calculate the stationary states of the laterally homogeneous charge carrier system for every lattice temperature. A necessary condition for a stationary state of the trapped hole density is given by a zero net increase rate in Eq. (8) when averaged over one period and over the longitudinal coordinate z,

$$\bar{R}_{p_t} = \frac{1}{L\tau}\int_t^{t+\tau} dt' \int_0^L dz[R_{pt}(z,t') - R_{nt}(z,t')] = 0, \tag{20}$$

as discussed in Ref. 26. To study the temperature dependence, we have calculated the stationary state at a given voltage and frequency as a function of the lattice temperature. For this purpose, we start a one-dimensional simulation at a constant lattice temperature $T_L=T_{\min}$ and calculate p_t after the system has converged to a stationary state. If T_L is sufficiently low, there is only a single stationary solution, and thus the result is independent of the initial condition. Taking the calculated p_t profile as a new initial condition, we increase the lattice temperature and let the system converge again to a stationary state and calculate p_t. We repeat this procedure up to a certain maximum value of $T_L=T_{\max}$. Since in the region of bistability, this yields only one of the two solutions, we then have to repeat the procedure by stepwise decreasing T_L until we reach again $T_{\min}$. The result of such a calculation for an applied voltage amplitude of U=110 V and a driving frequency of f=10 kHz is plotted in Fig. 3 (solid line). Here, the trapped hole density profile $p_t(z)$ has been characterized by its average value of $\bar{p}_t$. Obviously the system exhibits only one stationary state for temperatures above 320 K and below 275 K. In between, the system has two stable stationary states. Because the calculated values of $\bar{p}_t$ describe the stable stationary states in the plane, it can be concluded that in the vicinity of the lines the net growth rate $\bar{R}_{p_t}$ is positive on the left of that line and negative on the right of it. Therefore, for each temperature T_L of the bistable interval the $\bar{p}_t$ axis is separated into a region where the system is attracted to the low state and a region where it is attracted to the high state. The border between these regions is given by an unstable stationary state. Because it is not possible to find the unstable stationary states of the charge carrier

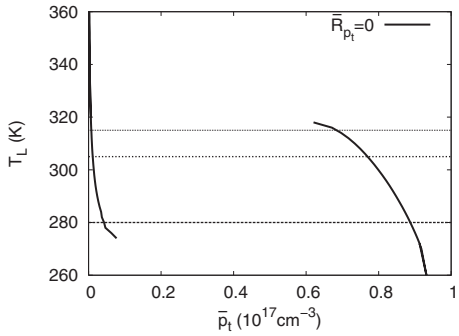

FIG. 3. Null cline diagram for the case of fixed lattice temperature. The $\bar{R}_{p_t}=0$ line connects the stable stationary states of the charge carrier system in the $\bar{p}_t$-T_L plane. The dotted lines indicate the temperatures shown in Fig. 2. Driving voltage: $U=110$ V, $f=10$ kHz.

system with our method, the exact position of this border line cannot be seen in the diagram, but it should connect the two stable lines to each other in some way.

Let us now explain our findings of the two-dimensional simulations in terms of the temperature dependence of the stationary states. At a lattice temperature of 280 K, we are close to the end of the lower branch in Fig. 3. Thus, the unstable stationary solution will be close to the low state, and a rather small perturbation will bring the system into the attractive region of the high state while very strong perturbations would be needed to drive the system from the high to the low state. In our case of an inhomogeneous initial condition, such perturbations are provided by the fronts between low and high states. Because of the large basin of attraction of the high state, this state will spread out, leading to moving fronts. Due to the periodic boundary conditions, the fronts eventually reach each other, resulting in a system that is completely in the high state, as has been found in Fig. 2(a). In contrast, at $T_L=315$ K, we are close to the end of the upper branch of the stationary profile. Thus, the unstable stationary solution will be close to the high state, resulting in a large basin of attraction of the low state. In this case, the low state will spread out, resulting in a collapse of the high state [see Fig. 2(c)]. As we have already seen above, between these values of the lattice temperature where the front velocities have opposite signs, there is one temperature where the front velocity vanishes. In the present case, this happens at approximately $T_L=305$ K. Evidently, at this temperature, the unstable stationary p_t profile should be approximately in the middle between the two stable ones.

B. Small frequencies, bistable mode

Let us now return to the full model including the effect of lattice heating. In general, Ohmic heating and heat transport lead to a spatially inhomogeneous and time-dependent lattice temperature profile which, in turn, influences the carrier dynamics. First, we are again interested in the number and stability of the stationary states of the laterally homogeneous system. In the last section, we identified these states as the intersections of the $\bar{R}_{p_t}=0$ line with the corresponding $T_L=$const line in a $\bar{p}_t$-T_L parameter plane.

In the present case of a spatially and temporally varying lattice temperature profile, the stationary state of the system also requires, in addition to a stationary value of $\bar{p}_t$, a stationary state of $\bar{T}_L$, the lattice temperature averaged with respect to one period, and the longitudinal coordinate z according to

$$\bar{T}_L(x,t)=\frac{1}{L\tau}\int_t^{t+\tau}dt'\int_0^L dz T_L(x,z,t'). \tag{21}$$

This temperature is stationary if the right hand side of Eq. (12) vanishes when averaged over t and z, i.e.,

$$\bar{R}_{T_L}=\frac{1}{L\tau}\int_t^{t+\tau}dt'\int_0^L dz\left[D_L\frac{\partial^2}{\partial z^2}T_L+\frac{e}{c_L\rho}(\mathbf{j}_p-\mathbf{j}_n)\cdot\mathbf{E}\right]=0. \tag{22}$$

We will refer to $\bar{R}_{T_L}$ as the net temperature increase rate. In the $\bar{T}_L$-$\bar{p}_t$ plane the stationary states are then characterized by the intersections of the lines $\bar{R}_{p_t}=0$ and $\bar{R}_{T_L}=0$. Such a diagram is generally called a null cline diagram,[34] and it will be the basis for the interpretation of the dynamical behavior in the present and in the following sections.

With a nonconstant lattice temperature, it is more complicated to calculate and plot a null cline diagram. We start the algorithm for calculating the $\bar{R}_{p_t}=0$ line exactly as we did it before by setting the lattice temperature on a constant value of T_L^0 and calculate the stationary states of the carrier system $p_t(T_L^0)$ in the temperature range $T_{\min}\leqslant T_L\leqslant T_{\max}$. Although the real temperature profiles are not exactly constant, this is a very good approximation due to the high diffusion constant and the slow reaction speed (compared to the driving period) of the lattice temperature. To obtain the $\bar{R}_{T_L}=0$ line, we start for each value of T_L^0 with the corresponding p_t profile in the temperature equation. Without changing the p_t profile, we then calculate the stationary solution of the lattice temperature equation, resulting in a temperature profile $T_L(p_t)$. At the end, we get for every temperature the stable stationary states of the carrier system, and for all stationary states of the carrier system we get a stationary state of the lattice temperature. If we characterize the state of the carrier system by the average density $\bar{p}_t$ and the lattice temperature profile (which is almost constant) by the temperature $\bar{T}_L$, we can plot the null clines in a $\bar{p}_t$-$\bar{T}_L$ plane. The results for a driving frequency of 10 kHz and two different driving voltages of 110 and 113 V are shown in Fig. 4 (solid and dashed lines). The horizontal dotted lines indicate the corresponding $v=0$ temperatures, i.e., the temperatures where a front between the low and the high state does not move. The stationary states of the system are given by the intersection of the $\bar{R}_{p_t}=0$ and $\bar{R}_{T_L}=0$ lines. Again, our method only allows us to obtain stable stationary states. The diagram thus shows that at both

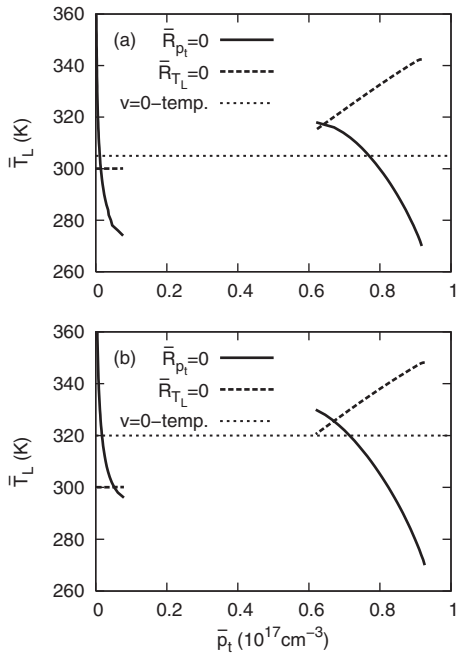

FIG. 4. Null cline diagram. The $\bar{R}_{p_t}=0$ line shows the stable stationary states of the charge carrier system, and the $\bar{R}_{T_L}=0$ line the stable stationary states of the lattice temperature. The $v=0$ temperature indicates the temperature where the velocity of the transition front between low- and high-state regions vanishes. Driving voltage: (a) $U=110$ V, $f=10$ kHz; (b) $U=113$ V, $f=10$ kHz.

voltages we have a bistable system and that the temperature of one stable state is lower than the $v=0$ temperature while the other is higher.

If we start a two-dimensional simulation with inhomogeneous initial conditions, as given by Eqs. (18a) and (18b), and a rather wide high-state interval $X=[16\ \mu\text{m}, 24\ \mu\text{m}]$ at an applied voltage amplitude of $U=110$ V and a frequency of $f=10$ kHz, the system exhibits a temporal evolution of the trapped hole density and the lattice temperature, as plotted in Figs. 5(a) and 5(b). The high-state region starts to shrink, reaches a minimal size after about 30 000 periods and then grows very slowly until it reaches a fixed size after about 60 000 periods. The lattice temperature, which has been taken to be homogeneously 300 K at the beginning, increases rapidly in the high-state region and converges with the trapped hole density to a stationary profile but, due to the strong diffusion process, the transition from high to low temperature is much less steep. If we start the system with a quite small initial high-state interval $X=[19\ \mu\text{m}, 21\ \mu\text{m}]$, we find a temporal evolution of the trapped hole density and the lattice temperature, as shown in Figs. 5(c) and 5(d). The high-state region initially grows very fast and finally converges to the same width as in the case of the initially wide high-state region. The lattice temperature also grows and ends up at the same profile that has been found before. Thus, under the present driving conditions, we observe the formation of a high-state filament with geometrical parameters that do not depend on the details of the initial condition.

We can explain this filament formation on the basis of the null cline structure in Fig. 4(a). Starting from its initial value

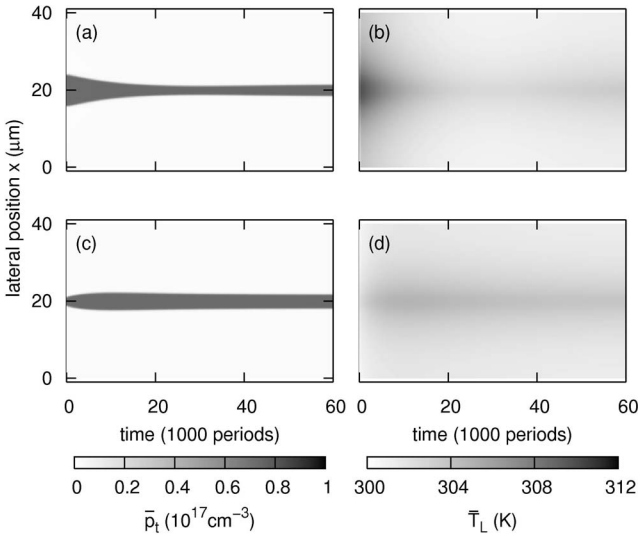

FIG. 5. Temporal evolution of the average trapped hole density [(a) and (c)] and the average lattice temperature [(b) and (d)] in a two-dimensional system, which started with two different inhomogeneous initial conditions. Driving voltage: $U=110$ V, $f=10$ kHz.

of 300 K, the lattice temperature in Fig. 5(b) rises very fast in the high-state region and causes temperatures at the transition fronts in Fig. 5(a), which are above the temperature at which the front velocity is zero. Consequently, the high-state area decreases. When the high-state area becomes smaller, the lattice temperature T_L at the transition fronts decreases and finally reaches the value at which the front speed vanishes. Then, the system converges into a stationary inhomogeneous state. The very small initial high-state region in Fig. 5(c), on the other hand, leads to a front temperature that gives rise to a front velocity with the opposite sign, i.e., directing toward the low-state region. The growing high-state region then causes the lattice temperature to rise and the front velocity to decrease until it drops to zero. Thus, due to this stabilization caused by the interplay between carrier dynamics and lattice temperature, a stationary filament with a well-defined size has been formed.

Figure 6 shows the temporal evolution of the system with identical initial conditions as in Figs. 5(c) and 5(d), but at a

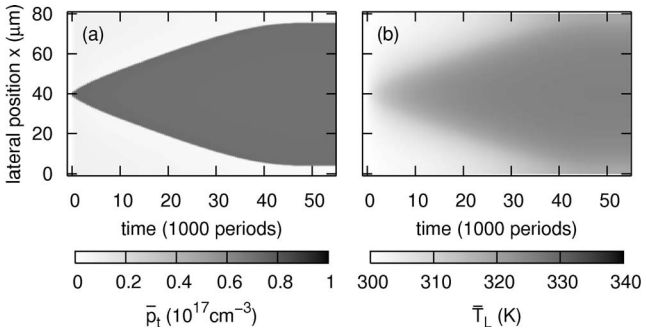

FIG. 6. Temporal evolution of the average trapped hole density (a) and the average lattice temperature (b) in a two-dimensional system, which started with inhomogeneous initial conditions. Driving voltage: $U=113$ V, $f=10$ kHz.

driving voltage amplitude of 113 V. Again, the high-state area increases, but now it increases until it almost covers the whole structure. Only when, due to the periodic boundary conditions, the moving fronts come sufficiently close to each other does the growth stop and a stationary state with a small low-state region remain. This behavior can again be understood on the basis of the corresponding null cline diagram plotted in Fig. 4(b). The main difference compared to the previous case is the fact that now the temperature of vanishing front speed is only slightly below the temperature of the high state. When going from the high-state to the low-state region the temperature decreases, and in the present case, at the front between these regions, it is lower than the $v=0$ temperature. Therefore, the fronts will move and the high-state region will grow. However, when one front approaches another one, due to the vicinity of the other high-state region, the temperature at the front increases until at a certain distance it reaches the $v=0$ temperature and the front will become stationary. Thus, a low-state filament (dark filament) is formed within a high-state region.

In both cases, we observe moving fronts, which reach a stationary state because of a repulsive interaction between two fronts. At small voltages, this repulsive interaction inhibits the complete collapse of a high-state region; instead, small solitary high-state regions with a stable size are formed. At higher voltages, a collapse of a low-state region is avoided, resulting in the formation of a small low-state region. Our results agree qualitatively with experimental findings, where at low driving frequencies and amplitudes isolated small luminescent spots have been observed and at higher amplitudes isolated areas of no luminescence were found.[6,17] The front velocity of approximately 20 μm/s is of the same order of magnitude as that reported in Ref. 8. However, it should be mentioned that there are also other experiments where much higher velocities up to 1000 μm/s were observed, for example, in Ref. 17.

C. High frequencies, oscillating mode

Complex patterns, such as spiral waves and target patterns, were found in various experiments when higher frequencies were applied. Obviously, it is not possible to simulate such patterns in a two-dimensional model; nevertheless, we can analyze the properties of our model under higher frequencies and answer the question whether such complex patterns should be expected in a three-dimensional model. For this purpose, we have performed calculations for the case of a driving frequency of 100 kHz.

To get an impression of the stationary states of the laterally homogeneous system, we first discuss the null cline diagrams plotted in Fig. 7 for the two voltages (a) 113 V and (b) 116 V. Let us first concentrate on the lower voltage [Fig. 7(a)]. In this case, we find only one stable stationary state, which has a low density of trapped holes and a lattice temperature below the $v=0$ temperature. Although the system is not bistable, we start the two-dimensional simulation with inhomogeneous initial conditions. Figure 8(a) shows the temporal evolution of an initially small high-state area ($X=[79\ \mu\text{m}, 81\ \mu\text{m}]$). Again, we find a stable high-current filament with a characteristic size. In the surroundings of a very small high-current area, the temperature [Fig. 8(b)] is almost equal to the low-state temperature, so the filament grows until the lattice temperature at the fronts is equal to the

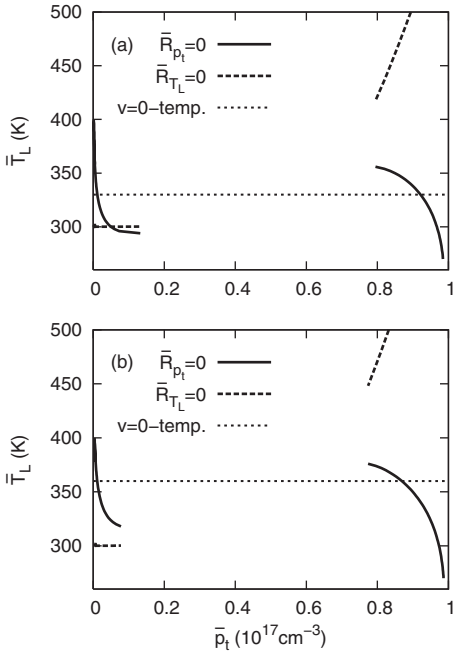

FIG. 7. Null cline diagram. The $\bar{R}_{p_t}=0$ line shows the stable stationary states of the charge carrier system, and the $\bar{R}_{T_L}=0$ line the stable stationary states of the lattice temperature. The $v=0$ temperature indicates the temperature where the velocity of the transition front between low- and high-state regions vanishes. Driving voltage: (a) $U=113$ V, $f=100$ kHz; (b) $U=116$ V, $f=100$ kHz.

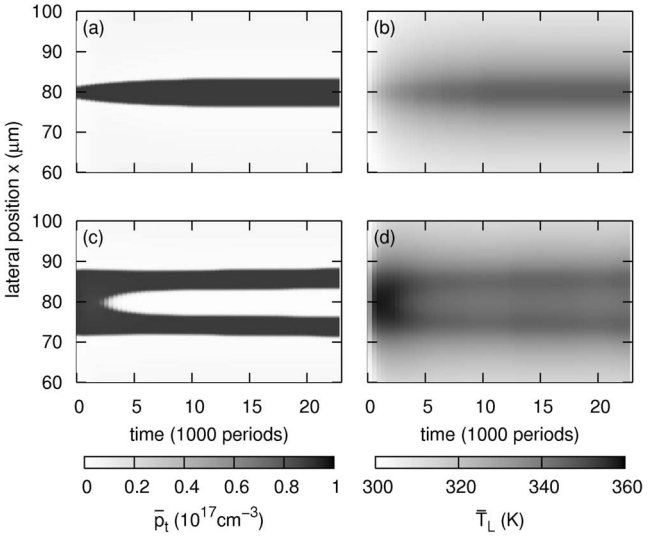

FIG. 8. Temporal evolution of the average trapped hole density [(a) and (c)] and the average lattice temperature [(b) and (d)] in a two-dimensional system, which started with two different inhomogeneous initial conditions. Note that only the central part of a total simulated lateral width of 160 μm is shown. Driving voltage: $U=113$ V, $f=100$ kHz.

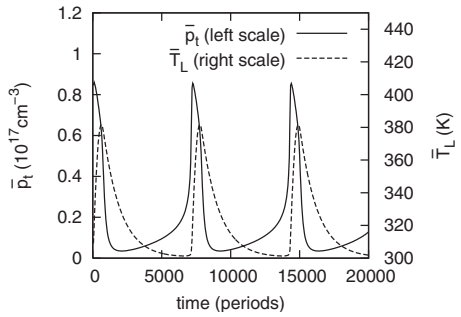

FIG. 9. Temporal evolution of the average trapped hole density and the lattice temperature obtained from a one-dimensional calculation. Driving voltage: $U=116$ V, $f=100$ kHz.

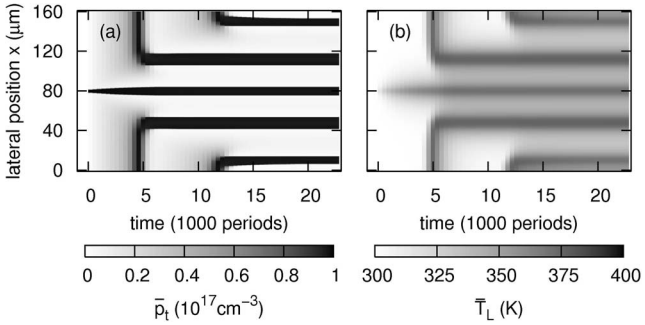

FIG. 10. Temporal evolution of the average trapped hole density (a) and the average lattice temperature (b) in a two-dimensional system, which started with inhomogeneous initial conditions. Driving voltage: $U=116$ V, $f=100$ kHz.

$v=0$ temperature. If we start the simulation with a large high-state area ($X=[72\ \mu\text{m}, 88\ \mu\text{m}]$), we find the temporal evolution shown in Figs. 8(c) and 8(d). Since there is no stable high state in the one-dimensional case, the almost homogeneous center of the high-state area switches to the low state. At the borders of the high-state area, however, the lattice temperature is not high enough to let the space charge vanish, and so two separated small high-state areas are build up. We find a weak repulsive interaction between these small areas, but the resulting movement can hardly be seen in Fig. 8(c). The reason for this interaction is a very small difference between the lattice temperatures at the outer and inner borders of the high-state regions.

A two-component system with a null cline diagram such as the one in Fig. 7(a) is often called an excitable medium. Such media are widely studied, and it was often reported that they can cause rotating wave patterns and other spatiotemporal patterns when the ratio of propagation velocities of the components is within a certain range.[35] We will come back to this point below.

Figure 7(b) shows the null cline diagram for an amplitude of 116 V. Here, we find no stable stationary state at all. Of course, there will be at least one intersection of the null clines in the unstable region corresponding to an unstable stationary state. However, the system will not stay in that state because even infinitesimally small perturbations will cause the system to leave that state. On the other hand, there is no other state the system could converge to. Systems with such a null cline diagram often show oscillatory dynamics when the system behaves as one dimensional, i.e., when it remains laterally homogeneous (see, e.g., Ref. 35). That this is indeed the case can be seen in Fig. 9, where we have plotted the average trapped hole density and the average lattice temperature as functions of time obtained from a one-dimensional calculation. We clearly see that if we start a simulation with a high state, the temperature rises and, because of the increased hole emission process, causes the trapped hole density to decrease. When the trapped hole density is low enough, the temperature decreases and, finally, the trapped hole density can rise again. For the present parameters, we find an oscillation period of approximately 7000 driving periods corresponding to about 70 ms.

If we start a two-dimensional simulation with inhomogeneous initial conditions ($X=[78\ \mu\text{m}, 81\ \mu\text{m}]$) at the same driving parameters, we find a temporal evolution of the system, as shown in Fig. 10. The high-state area in the middle does not vanish because the temperature diffusion effect drops the local temperature to the $v=0$ value. The homogeneous areas around this filament change from low to high state. However, in a small region around the original filament, the temperature is higher, which inhibits this switching to the high state. The temperature in the high-state region then starts to grow, resulting in a switching back to the low state, as seen in the one-dimensional calculations. However, small regions at the edges of the high-state area have a lower lattice temperature, and so they will remain in a high state. Thus, two new filaments have been formed on each side of the initial filament. This process repeats until the whole area is covered by a spatially periodic pattern of filaments. As a result of this process, it should be expected that a three-dimensional simulation of the system might show concentric rings of different sizes. This would fit to the so called target patterns, which have been reported in Ref. 6.

IV. SMALL TEMPERATURE DIFFUSION CONSTANT

One important parameter of two-component reaction-diffusion models is the ratio of the propagation velocities. There are indications from some experiments that the propagation velocity of the charge carrier system is somehow influenced by driving and preparation parameters of the MISIM structure. Indeed, measured front velocities range from about 10 μm/s (Ref. 8), in agreement with our results to more than 1000 μm/s (Ref. 17). Increasing the characteristic lateral velocities of the charge carrier system would require modifications in the transport model, e.g., by adding surface diffusion processes. Such an extension is beyond the scope of the present paper. However, we can study the influence of the ratio between the characteristic velocities of the carriers and the temperature by changing the temperature diffusion constant. For this purpose, in the present section, we have lowered the lattice heat conductivity by 3 orders of magnitude to a value of $\kappa=17\times10^{-3}$ W/m K.

The one-dimensional behavior of the system remains approximately the same as for the original heat conductivity. So, at a frequency of $f=100$ kHz, we find again the null cline

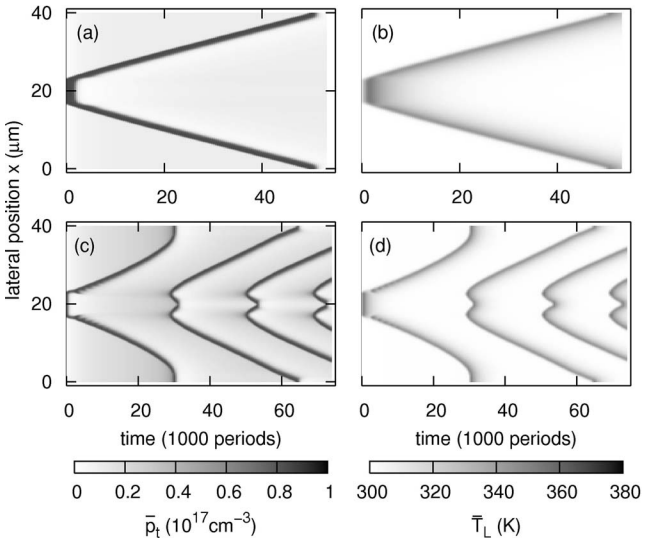

FIG. 11. Temporal evolution of the average trapped hole density [(a) and (c)] and the average lattice temperature [(b) and (d)] in a two-dimensional system with reduced temperature diffusion coefficient, which started with inhomogeneous initial conditions. Driving voltage: [(a) and (b)] $U=113$ V, $f=100$ kHz; [(c) and (d)] $U=114.5$ V, $f=100$ kHz.

diagram of an excitable and an oscillatory medium at small and high voltage amplitudes, respectively. Only the slope of the $\bar{R}_{T_L}=0$ lines at high $\bar{p}_t$ values increases slightly due to the slower heat transport. However, if we start two-dimensional simulations with inhomogeneous initial conditions, we find considerably modified results. Figure 11(a) shows the temporal evolution of an initially small high-state interval ($X=[18\ \mu\text{m}, 22\ \mu\text{m}]$) in the case of an excitable medium ($U=113$ V). Again, the almost homogeneous center of the high-state region switches to the low state. Because of the small temperature diffusion constant, the lattice temperature at the borders is lower than the $v=0$ temperature [Fig. 11(b)], and so the fronts start to move toward the low-state regions and to heat the lattice at the regions that are switched into the high state. Because of the absence of a stable high state in the one-dimensional simulation, the heated regions switch back to the low state, and so two moving high-state pulses appear, which are both followed by high temperature pulses. When these two pulses collide with each other at the borders of the simulation area, they annihilate each other. This type of dynamics resembles the solitary ring-shaped waves, which have been observed by Zuccaro *et al.*[6] On the other hand, this kind of dynamics can also cause rotating wave patterns,[35] which have been found, for example, by Rüfer *et al.*[17]

We find another interesting spatiotemporal behavior when we use the same initial conditions but a slightly larger voltage amplitude of 114.5 V, where the null clines do not exhibit a stable stationary state in the one-dimensional simulation but show an oscillatory dynamics with an oscillation period of approximately 31 000 driving periods. Figure 11(c) shows that in the beginning we find a similar situation as in Fig. 11(a), but after a while the core of the initial high-state region switches back from the low to the high state and sends out another pair of traveling high-state pulses. Finally, this causes a traveling wave train created by the oscillating core. This behavior is qualitatively similar to the series of ring waves sent out periodically by a core, which has been observed by Vlasenko *et al.*[27]

V. CONCLUSIONS

We have analyzed the formation and dynamics of transverse patterns in ac-driven ZnS:Mn thin-film electroluminescent devices. Based on a material- and structure-specific model for the carrier dynamics in the semiconductor layer, we have found a variety of different static or dynamic patterns, and we have studied the influence of different driving and material parameters on their dynamical behavior. The physics of the pattern formation is closely related to a delicate interplay between space charges and the local lattice temperature: High-current regions are associated with large space charges due to the trapping of holes generated by impact ionization processes; high currents, on the other hand, lead to a strong Joule heating of the lattice, which increase the thermal emission of holes from the trap states and thus reduce the space charge. This interplay reflects itself in the null cline diagram in the space of spatially averaged space charges and lattice temperatures, which is therefore well suited for the interpretation of the numerically obtained pattern dynamics.

To describe the interaction of carrier transport and lattice heating in ZnS:Mn thin-film electroluminescent structures, two-dimensional transport equations for the charge carrier system and for the lattice temperature have been formulated. The number and stability of stable stationary states of the one-dimensional system have been determined by calculating null cline diagrams for different frequencies and amplitudes of the applied voltage. By numerical simulations, the temporal evolution in a two-dimensional system after inhomogeneous initial conditions has been calculated for different parameters.

For low frequencies, we found from the null cline diagram that the system is bistable in a wide range of voltage amplitudes. Here, in a two-dimensional simulation, the given inhomogeneous initial conditions give rise to either a small stable high-state area in a low-state system or vice versa, corresponding to a bright or dark filament. The width of these filaments is found to be independent of the initially given widths of the regions. This fits to experimental observations, where two different inhomogeneous scenarios have been observed at low frequencies: small luminescent spots called filaments at lower amplitudes and isolated dark areas in a bright background at higher amplitudes.

At high frequencies, the null clines show either only a single stable stationary state (for small voltage amplitudes) or no stable stationary state at all (for higher amplitudes). For small amplitudes, the null cline diagram corresponds to the typical situation of excitable media. The two-dimensional simulation with inhomogeneous initial conditions results again in small stable high-state areas; however, they evolve in a different way from the inhomogeneous initial condition.

For a reduced value of the lattice heat conductivity, also dynamical patterns like moving pulses show up.

A system with only an unstable stationary state exhibits an oscillatory behavior in a one-dimensional simulation. In a two-dimensional simulation with inhomogeneous initial conditions, it leads to spatially periodic patterns in a qualitative agreement with the experimentally observed target patterns. For a low value of the lattice heat conductivity, we observe periodic traveling pulses, which are sent out by a core.

In conclusion, we have demonstrated that the model presented in this paper exhibits a variety of stable stationary and nonstationary spatially inhomogeneous solutions when varying the driving and/or material parameters. An extension of this model to three spatial dimensions could be an important step toward finding and explaining pattern formation in ZnS:Mn thin-film devices.

ACKNOWLEDGMENTS

The authors wish to thank S. Zuccaro, H.-G. Purwins (University of Münster, Germany), and N. A. Vlasenko (Institute of Semiconductor Physics, Kiev, Ukraine) for many fruitful discussions.

[1] Y. Ono, *Electroluminescent Displays* (World Scientific, Singapore, 1995).
[2] V. Marello, W. Rühle, and A. Onton, Appl. Phys. Lett. **31**, 452 (1977).
[3] W. Rühle, V. Marrello, and A. Onton, J. Electron. Mater. **8**, 839 (1979).
[4] A. I. Beletskii and N. A. Vlasenko, Tech. Phys. Lett. **19**, 13 (1993).
[5] A. I. Beletskii and N. A. Vlasenko, Tech. Phys. Lett. **19**, 798 (1993).
[6] S. Zuccaro, F.-J. Niedernostheide, B. Kukuk, M. Strych, and H.-G. Purwins, Phys. Rev. E **62**, 1284 (2000).
[7] N. A. Vlasenko, H.-G. Purwins, V. M. Popov, I. A. Gumenyuk, A. S. Klimenko, Y. F. Kononets, F.-J. Niedernostheide, L. I. Veligura, and S. Zuccaro, Phys. Status Solidi A **194**, 237 (2002).
[8] N. A. Vlasenko, H.-G. Purwins, Z. L. Denisova, Y. F. Kononets, F.-J. Niedernostheide, L. I. Veligura, and S. Zuccaro, Semicond. Phys., Quantum Electron. Optoelectron. **7**, 82 (2004).
[9] E. Schöll, *Nonlinear Spatio-Temporal Dynamics and Chaos in Semiconductors* (Cambridge University Press, Cambridge, UK, 2001).
[10] L. I. Bonilla and H. T. Grahn, Rep. Prog. Phys. **68**, 577 (2005).
[11] A. Wacker, Phys. Rep. **357**, 1 (2002).
[12] X. R. Wang and Q. Niu, Phys. Rev. B **59**, R12755 (1999).
[13] Z. Z. Sun, H. T. He, J. N. Wang, S. D. Wang, and X. R. Wang, Phys. Rev. B **69**, 045315 (2004).
[14] E. Schöll, *Nonequilibrium Phase Transitions in Semiconductors* (Springer, Berlin, 1987).
[15] F.-J. Niedernostheide, M. Ardes, M. Or-Guil, and H.-G. Purwins, Phys. Rev. B **49**, 7370 (1994).
[16] M. Meixner, P. Rodin, E. Schöll, and A. Wacker, Eur. Phys. J. B **13**, 157 (2000).
[17] H. Rüfer, V. Marrello, and A. Onton, J. Appl. Phys. **51**, 1163 (1980).
[18] W. E. Howard, O. Sahni, and P. M. Alt, J. Appl. Phys. **53**, 639 (1982).
[19] K. A. Neyts, D. Corlatan, P. De Visschere, and J. Van den Bossche, J. Appl. Phys. **75**, 5339 (1994).
[20] K. A. Neyts and P. De Visschere, J. Appl. Phys. **68**, 4163 (1990).
[21] E. Bringuier, Philos. Mag. B **75**, 209 (1997).
[22] M. Beale, Philos. Mag. B **68**, 573 (1993).
[23] S. Zuccaro, T. Raker, F.-J. Niedernostheide, T. Kuhn, and H.-G. Purwins, Chaos, Solitons Fractals **17**, 231 (2000).
[24] T. D. Thompson and J. W. Allen, J. Phys. C **20**, L499 (1987).
[25] A. Kuligk, N. Fitzer, and R. Redmer, Phys. Rev. B **71**, 085201 (2005).
[26] K. Meyer, T. Raker, F.-J. Niedernostheide, and T. Kuhn, Semicond. Sci. Technol. **21**, 565 (2006).
[27] N. A. Vlasenko, Z. L. Denisova, L. I. Veligura, S. Zuccaro, F.-J. Niedernostheide, and H.-G. Purwins, J. Cryst. Growth **214-215**, 944 (2000).
[28] E. Bringuier, J. Appl. Phys. **66**, 1314 (1989).
[29] M. Lundstrom, *Fundamentals of Carrier Transport* (Cambridge University Press, Cambridge, 2000).
[30] T. Raker, T. Kuhn, A. Kuligk, N. Fitzer, R. Redmer, S. Zuccaro, F.-J. Niedernostheide, and H.-G. Purwins, Physica B **314**, 185 (2002).
[31] W. Shockley and W. T. Read, Phys. Rev. **87**, 835 (1952).
[32] S. Sze, *Physics of Semiconductor Devices* (Wiley, New York, 1981).
[33] N. Fitzer, A. Kuligk, R. Redmer, M. Städele, S. M. Goodnick, and W. Schattke, Phys. Rev. B **67**, 201201(R) (2003).
[34] A. S. Mikhailov, *Foundations of Synergetics I* (Springer, Berlin, 1994).
[35] J. D. Murray, *Mathematical Biology* (Springer, Berlin, 1989).